# Acoustic wavefield imaging using the energy norm

*Daniel Rocha*[1]*, Nicolay Tanushev*[2] *& Paul Sava*[1]
[1]*Center for Wave Phenomena, Colorado School of Mines and* [2]*Z-Terra, Inc.*

## SUMMARY

Wavefield energy can be measured by the so-called *energy norm*. Using this norm, we propose an imaging condition that represents the total reflection energy and accounts for wavefield directionality in space-time, thus enabling us to attenuate backscattering artifacts in reverse-time migration (RTM). This imaging condition has the flexibility to attenuate any selected angle, and by exploiting this property, we develop a procedure to emphasize events such as backscattered, diving and head waves, with application to full waveform inversion (FWI). This application involves filtering the FWI gradient to preserve its tomographic term consisting of waves propagating along the same path, while attenuating the migration term consisting of waves crossing at arbitrary propagation directions.

## INTRODUCTION

Reverse-time migration (RTM) uses cross-correlation of extrapolated source and receiver wavefields to form an image (Clærbout, 1985). Similarly, full waveform inversion (FWI) uses cross-correlation of extrapolated state and adjoint wavefields to form the gradient of an objective function used for optimization (Tarantola, 1984; Hindlet and Kolb, 1988; Plessix, 2006). In both cases, cross-correlation produces undesirable events in the image, or in the gradient. For example, waves propagating in the same direction and overlapping at all locations and all times (backscattered waves, diving waves) lead to artifacts in RTM images (Diaz and Sava, 2015). Similarly, cross-correlation of waves propagating in arbitrary directions in state and adjoint wavefields lead apparent reflections that corrupt the reconstructed gradients.

Alternatives to crosscorrelation have been investigated for both RTM and FWI (Chang and McMechan, 1986; Fletcher et al., 2005; Gao et al., 2012). For RTM, backscattering artifacts can be attenuated with a Laplacian filter applied after the imaging condition. Other post-imaging filtering techniques are reported in the literature (Guitton et al., 2007; Xu et al., 2014). This filtering can also be applied prior to imaging by using the propagation directions of wavefields obtained by Poynting vectors (Yoon and Marfurt, 2006; Costa et al., 2009) or by wavefield decomposition (Suh and Cai, 2009; Liu et al., 2011) to attenuate wavefields traveling in the same direction. Similarly, we can preserve the FWI tomographic component using filtering of the gradient (Almomin and Biondi, 2012; Albertin et al., 2013; Tang et al., 2013; Alkhalifah, 2015). All of these approaches use an extension of the gradient, similar to extended images in wave-equation migration (Sava and Fomel, 2006; Sava and Vasconcelos, 2011), to separate tomographic and migration components by exploiting the angle between the wave vectors. We define the 4D vector fields based on the energy norm, emphasizing the total wavefield energy which is invariant as a function of space and time.

We seek a form of wavefield comparison (an imaging condition) that directly exploits the directionality of the wavefields in the 4D space-time space. We achieve this by transforming the extrapolated scalar wavefields into 4D vector fields that capture their directionality and enable us to filter undesirable events. The proposed imaging condition is also discussed by Tarantola (1984) in the context of waveform inversion using impedance as the model parameter. This imaging condition attenuates the backscattering and is related to the Laplacian filter, as shown by other authors (Douma et al., 2010; Whitmore and Crawley, 2012; Pestana et al., 2013; Brandsberg-Dahl et al., 2013; Sun and Wang, 2013). Although more general in nature, the imaging condition is ideally suited for backscattering filtering.

## REVERSE-TIME MIGRATION

For a given seismic experiment with index $e$, we consider the wavefield $W(e,\mathbf{x},t)$ as a solution to the acoustic wave-equation

$$\frac{\partial^2 W}{\partial t^2} - v^2\nabla^2 W = f\,. \tag{1}$$

One can define a measure of energy for a solution to the homogeneous acoustic wave-equation within a spatial domain $\Omega$ (Evans, 1997; McOwen, 2003) as

$$E(t) = \frac{1}{2}\int_{\Omega}\left[\frac{1}{v^2}\left(\frac{\partial W}{\partial t}\right)^2 + |\nabla W|^2\right] d\mathbf{x}\,. \tag{2}$$

The time derivative term corresponds to the kinetic energy of the wavefield, and the spatial gradient term corresponds to its potential energy. The wavefield energy is conserved over time as seen by taking the derivative of equation 2 with respect to time.

Considering equation 2 as a norm, we can define an inner-product for two wavefields $U(e,\mathbf{x},t)$ and $V(e,\mathbf{x},t)$:

$$\langle U,V\rangle_E = \sum_{e,\mathbf{x},t}\left(\frac{1}{v}\frac{\partial U}{\partial t}\frac{1}{v}\frac{\partial V}{\partial t} + \nabla U\cdot\nabla V\right)\,. \tag{3}$$

The inner-product in equation 3 is composed of the dot product between the gradient vectors of the wavefields plus the product of their time derivatives scaled by the slowness $(1/v)$. The time dimension provides an additional derivative component beyond the components of the spatial gradient. Thus, a wavefield $W(e,\mathbf{x},t)$ can be represented in a Euclidean space with spatial coordinates $\mathbf{x}=\{x,y,z\}$ and an additional coordinate $vt$. The gradient of $W$ in this four-dimensional space can be defined as follows:

$$\left(\frac{\partial W}{\partial x},\frac{\partial W}{\partial y},\frac{\partial W}{\partial z},\frac{1}{v}\frac{\partial W}{\partial t}\right)\,. \tag{4}$$

This vector indicates the space and time directionality of the wavefield at a particular position and time. This notion of a four-dimensional gradient is used in other research areas, such as special relativity and wave theory, with the following compact notation (Feynman et al., 1964; Chappel et al., 2010):

$$\Box W = \left(\nabla W,\frac{1}{v}\frac{\partial W}{\partial t}\right)\,. \tag{5}$$

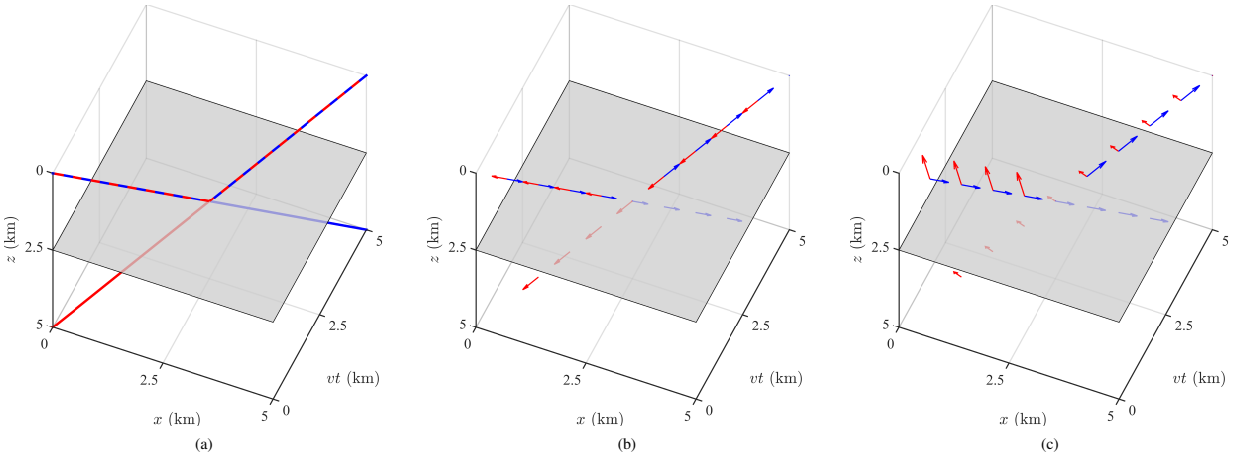


Figure 1: Schematic representation of the imaging conditions, with a horizontal reflector. Blue lines/arrows indicate the source wavefield, and red lines/arrows indicate the receiver wavefield. (a) Conventional imaging condition (cross-correlation of extrapolated wavefields), (b) imaging condition in equation 6, and (c) imaging condition in equation 13. In (c), backscattered wavefields are characterized by orthogonal vectors $\square U$ and $\square V$.

If the inner product in equation 3 is evaluated at each spatial location, we can define an imaging condition as

$$\begin{aligned} I_E &= \sum_{e,t} \square U \cdot \square V \,, \\ &= \sum_{t} \left( \frac{1}{v}\frac{\partial U}{\partial t}\frac{1}{v}\frac{\partial V}{\partial t} + \nabla U \cdot \nabla V \right) . \end{aligned} \tag{6}$$

We refer to equation 6 as the energy imaging condition, which forms an image at every location where the dot product between the vectors $\square U$ and $\square V$ is nonzero.

In the Fourier domain, the vectors $\square U$ and $\square V$ are:

$$\widetilde{\square W} = i\left(\mathbf{k}, -\frac{\omega}{v}\right)\tilde{W} \,. \tag{7}$$

Therefore, the dot product between $\widetilde{\square U}$ and $\widetilde{\square V}$ is

$$\begin{aligned} \widetilde{\square U} \cdot \widetilde{\square V} &= \left[ -\mathbf{k}_s \cdot \mathbf{k}_r + \frac{\omega^2}{v^2} \right] \tilde{U}\tilde{V}^* \\ &= \left[ -||\mathbf{k}_s||||\mathbf{k}_r|| \cos(2\theta) + \frac{\omega^2}{v^2} \right] \tilde{U}\tilde{V}^* \,, \end{aligned} \tag{8}$$

where $2\theta$ is the reflection angle and also the angle between the spatial gradient vectors. Replacing the dispersion relation of the acoustic wave equation in equation 8 leads to

$$\widetilde{\square U} \cdot \widetilde{\square V} = \left[ -\frac{\omega^2}{v^2}\cos(2\theta) + \frac{\omega^2}{v^2} \right] \tilde{U}\tilde{V}^* \,. \tag{9}$$

Equation 9 enables us to attenuate a certain reflection of angle $\theta_c$ by applying a scaling factor to the second term, thus nullifying the term in the brackets:

$$\widetilde{\square U} \cdot \widetilde{\square V} = \left[ -\frac{\omega^2}{v^2}\cos(2\theta) + \frac{\omega^2}{v^2}\cos(2\theta_c) \right] \tilde{U}\tilde{V}^* \,. \tag{10}$$

We can rewrite equation 8 as

$$\widetilde{\square U} \cdot \widetilde{\square V} = \left[ \frac{\omega^2}{v^2}\cos(2\theta_c) - \mathbf{k}_s \cdot \mathbf{k}_r \right] \tilde{U}\tilde{V}^* \,. \tag{11}$$

Therefore, we can modify the imaging condition in equation 6 by including the angle factor $\cos(2\theta_c)$

$$I_E = \sum_{e,t} \left( \cos(2\theta_c)\frac{1}{v}\frac{\partial U}{\partial t}\frac{1}{v}\frac{\partial V}{\partial t} + \nabla U \cdot \nabla V \right) . \tag{12}$$

In order to attenuate backscattering events, characterized by angle $2\theta_c = 180°$, we can rewrite the imaging condition:

$$I_E = \sum_{t} \left( -\frac{1}{v}\frac{\partial U}{\partial t}\frac{1}{v}\frac{\partial V}{\partial t} + \nabla U \cdot \nabla V \right) . \tag{13}$$

One can show the imaging condition in equation 13 is related to the Laplacian filter by

$$I_E = \frac{1}{2}\nabla^2 I_{L_2} \,. \tag{14}$$

Therefore, the proposed imaging condition is the general form of the filtering using the Laplacian operator for any reflection angle $\theta_c$.

We illustrate the imaging condition in equation 13 with a 2-D theoretical experiment depicted in Figure 1. The rays from source and receiver wavefields are represented in this space-time continuum with red and blue lines, respectively. Backscattering is represented by dashed lines. The conventional imaging condition (Figure 1a) forms an image at all locations above the reflector where the wavefields coexist. The imaging conditions in equations 6 and 13 depicted in Figures 1b and 1c, respectively, use the 4D vectors fields $\square U$ and $\square V$. As the vectors corresponding to backscattering events are orthogonal in Figure 1c, they do not contribute to the image formed by the imaging condition in equation 13.

The angle between $\square U$ and $\square V$ influences the amplitude of the energy image. Using $I_E$ from equation 11 for the special case when $\cos(2\theta_c) = -1$, we have

$$I_E(\mathbf{k}) = -\sum_{e,\omega} \left[ 1 + \cos(2\theta) \right] \frac{\omega^2}{v^2}\tilde{U}\tilde{V}^* \,. \tag{15}$$

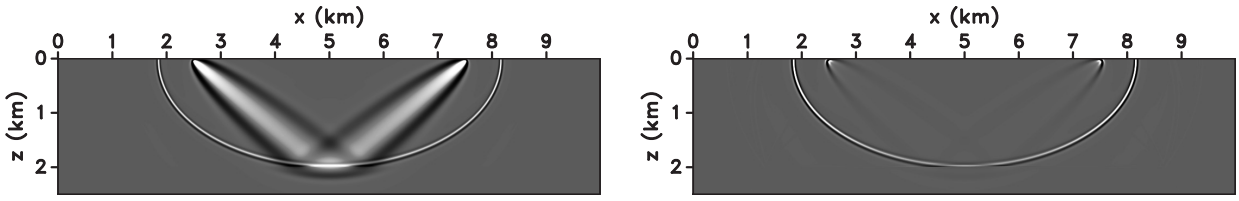


Figure 2: Experiment with a flat reflector, one source and one receiver on the surface at the locations $x = 2.5$ km and $x = 7.5$ km, respectively: (a) conventional image and (b) energy image.

Following the strategy from Zhang and Sun (2009), we can preserve the phase of the image by integrating the source function and receiver data before wavefield extrapolation, which means scaling $I_E$ by $\frac{1}{\omega^2}$ in the frequency domain; after the imaging condition, one can multiply the image by $v^2(\mathbf{x})$ at each spatial location. The amplitude of the resulting image is a function of the reflection angle by the term $1+\cos(2\theta)$. This is also true for the Laplacian filter, and we can obtain the same expression from Zhang and Sun (2009) starting from equation 14:

$$-\sum_{\omega} 2\left[1+\cos\left(2\theta\right)\right]\frac{\omega^2}{v^2}\tilde{U}\tilde{V}^* = -||\mathbf{k}||^2\sum_{\omega}\tilde{U}\tilde{V}^*\,, \qquad (16)$$

where

$$||\mathbf{k}||^2 = \frac{4\omega^2\cos^2\left(\theta\right)}{v^2}\,, \qquad (17)$$

which demonstrates that the Laplacian filter applied to RTM images depends on the reflection angle $\theta$.

Another particular case is when the energy imaging condition is used to attenuate normal-incidence reflections ($\cos(2\theta_c) = 1$). Using equation 11 and trigonometric relations, we obtain the following pair of imaging conditions:

$$I_E\left(\mathbf{k},\theta_c=0^\circ\right) \quad = \quad +2\sum_{e,\omega}\sin^2(\theta)\frac{\omega^2}{v^2}\tilde{U}\tilde{V}^*\,, \qquad (18)$$

$$I_E\left(\mathbf{k},\theta_c=90^\circ\right) \quad = \quad -2\sum_{e,\omega}\cos^2(\theta)\frac{\omega^2}{v^2}\tilde{U}\tilde{V}^*\,. \qquad (19)$$

For illustration, Figure 2 shows a simple constant velocity experiment with a flat reflector at $z = 2$km, and with one source and one receiver on the surface at $x = 2.5$km and $x = 7.5$km, respectively. As expected, the conventional image (Figure 2a) shows backscattering artifacts, which are strong along the path at 45° reflection angle. The energy image in Figure 2b effectively attenuates the backscattering artifacts. Likewise, Figures 3a-3b show the application of the proposed imaging condition on the Sigsbee model. The conventional image in Figure 3a is masked by the low frequency backscattered energy; in contrast, the energy image removes all low frequency artifacts in Figure 3b.

## FULL WAVEFORM INVERSION

The imaging condition in equations 18 enables us to select a range of reflection angles with maximum amplitude at 90°. However, the image $I_E\left(\mathbf{k},\theta_c=0^\circ\right)$ selects a broad range of reflection angles. A suitable option to make this range narrower is to apply an exponential function that has the greatest decay for angles far from 90°. The complementary image $I_E\left(\mathbf{k},\theta_c=90^\circ\right)$ indicates how far a certain angle is from 90°. Thus, we can define an image filtered by an exponential function applied to $I_E\left(\mathbf{k},\theta_c=0^\circ\right)$ as

$$I_E^{tomo} = I_E\left(\mathbf{k},\theta_c=0^\circ\right)e^{-aI_E\left(\mathbf{k},\theta_c=90^\circ\right)}\,, \qquad (20)$$

where $I_E^{tomo}$ stands for the tomographic component of the image. The image inside the exponential should be normalized, such that only the $\sin^2\left(\theta\right)$ factor is accounted for in the exponential. Filtering the image $I_E\left(\mathbf{k},\theta_c=0^\circ\right)$ using the complementary image $I_E\left(\mathbf{k},\theta_c=90^\circ\right)$, equations 18 and 19, is applicable to the source and receiver wavefields at each time step, as well.

We investigate the efficiency of the proposed FWI gradient filtering with a simple model with a true velocity of 2.5km/s. The geometry consists of one source at $x = 1$km and one receiver at $x = 5$km, both at depth $z = 2.25$km. The initial velocity used is 20% higher than the true velocity. Crosstalk artifacts are visible in the conventional gradient (Figure 4a). The energy gradients filtered in the image domain (Figures 4b) and wavefield domain (4c) show attenuated reflections and decreased amplitude for wide-angle reflections.

## CONCLUSIONS

The energy imaging condition provides an elegant and effective procedure for attenuating backscattering artifacts in reverse-time migration; this method generates an image representing the projection of four-dimensional space-time vectors ($\Box U$ and $\Box V$) onto one-another. Our new imaging condition explains the effectiveness of the Laplacian operator in attenuating events corresponding to waves propagating along the same path, but can be used to attenuate waves at arbitrary reflection angles. The new imaging condition can also be used to generate complementary images as a function of incidence and reflection angles, which enables us to filter the FWI gradient in order to attenuate its reflection components and favor the transmission (tomographic) component.

## ACKNOWLEDGEMENTS

We thank the sponsor companies of the Consortium Project on Seismic Inverse Methods for Complex Structures, whose support made this research possible. The reproducible numeric examples in this paper use the Madagascar open-source software package (Fomel et al., 2013) freely available from http://www.ahay.org.

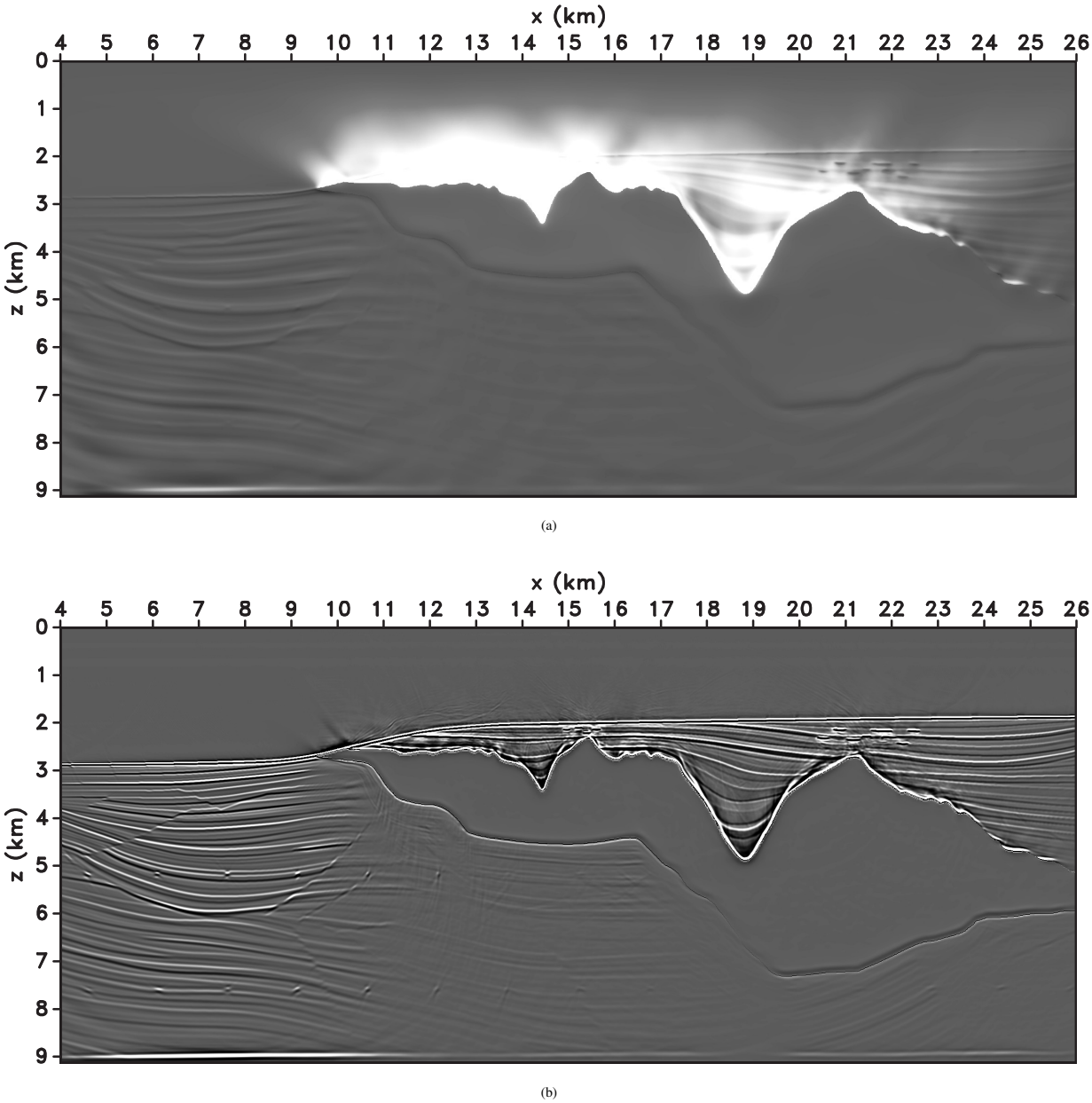


Figure 3: Sigsbee migration: (a) conventional image, and (b) energy image.

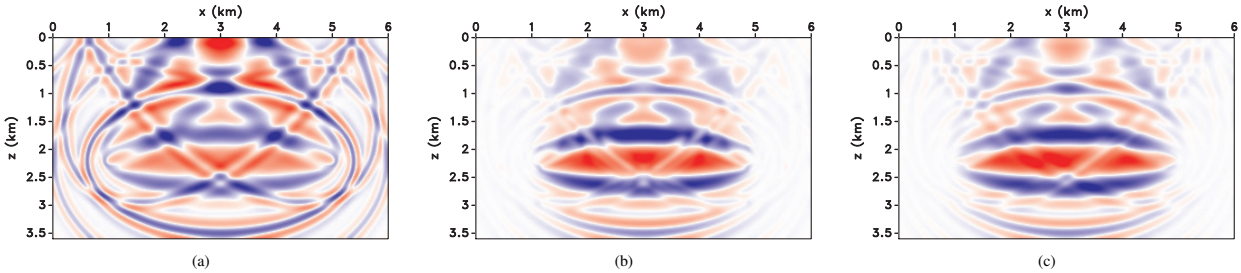


Figure 4: Filtering the FWI gradient using equation 20. (a) Conventional FWI gradient, (b) energy filtered FWI gradient, with the exponential filter applied on the image, and (c) on the wavefields. The free surface generates artifacts in the gradient. Most of the reflection artifacts are attenuated.